N^6-methyladenosine (m^{6}A) recruits and repels proteins to regulate mRNA homeostasis

Raghu R Edupuganti[1,4], **Simon Geiger**[2,4], **Rik G H Lindeboom**[1,4], **Hailing Shi**[3,4], **Phillip J Hsu**[3], **Zhike Lu**[3], **Shuang-Yin Wang**[1], **Marijke P A Baltissen**[1], **Pascal W T C Jansen**[1], **Martin Rossa**[2], **Markus Müller**[2], **Hendrik G Stunnenberg**[1], **Chuan He**[3], **Thomas Carell**[2], and **Michiel Vermeulen**[1]

[1]Department of Molecular Biology, Faculty of Science, Radboud Institute for Molecular Life Sciences, Radboud University Nijmegen, Nijmegen, the Netherlands [2]Center for Integrated Protein Science at the Fakultät für Chemie und Pharmazie, Ludwig-Maximilians-Universität München, Munich, Germany [3]Department of Chemistry, Department of Biochemistry and Molecular Biology, and Institute for Biophysical Dynamics, Howard Hughes Medical Institute, The University of Chicago, Chicago, Illinois, USA

Abstract

RNA modifications are integral to the regulation of RNA metabolism. One abundant mRNA modification is N^6-methyladenosine (m^{6}A), which affects various aspects of RNA metabolism, including splicing, translation and degradation. Current knowledge about the proteins recruited to m^{6}A to carry out these molecular processes is still limited. Here we describe comprehensive and systematic mass-spectrometry-based screening of m^{6}A interactors in various cell types and sequence contexts. Among the main findings, we identified G3BP1 as a protein that is repelled by m^{6}A and positively regulates mRNA stability in an m^{6}A-regulated manner. Furthermore, we identified FMR1 as a sequence-context-dependent m^{6}A reader, thus revealing a connection between an mRNA modification and an autism spectrum disorder. Collectively, our data represent a rich resource and shed further light on the complex interplay among m^{6}A, m^{6}A interactors and mRNA homeostasis.

m[6]A was first recognized as an abundant eukaryotic mRNA modification in the 1970s[1,2], but the functional significance of this modification remained unclear for years. Recently, it was shown that m[6]A is enzymatically added to and removed from mRNA molecules[3–5]. A heterodimer of METTL3–METTL14, in complex with WTAP, KIAA1429 and ZFP217, catalyzes the addition of a methyl group to adenosine in the context of a conserved consensus sequence (ACU)[5–8]. Two demethylases, FTO and ALKBH5, are known to remove the m[6]A modification[3,4]. Furthermore, researchers have used antibody-based enrichment methods to determine the transcriptome-wide distribution of m[6]A[9,10]. m[6]A marks several thousand mRNAs in mammalian cells and is enriched at the translation-termination region[9,10]. In recent years, various biological phenomena have been associated with the m[6]A modification on mRNA, such as obesity[11], plant development[12], yeast meiosis[13], cancer[14,15], cell fate transitions[16], fertilization[17] and pluripotency[18]. At the molecular level, m[6]A is known to affect mRNA stability[19], translation[20–22], microRNA biogenesis[23], splicing[11,24], X-chromosome inactivation[25] and other biological processes[26].

One important question is how m[6]A affects mRNA homeostasis. Previous work has shown that the YTH domain is a specific 'm[6]A-reader' domain[9], suggesting that YTH-domain-containing proteins act as effectors of m[6]A in cells. Indeed, recent studies have revealed a role for YTH-domain-containing proteins in the regulation of various aspects of mRNA homeostasis: YTHDF2 regulates mRNA stability[19], YTHDC1 regulates splicing[24], and YTHDF1 and YTHDF3 regulate translation[22,27]. In addition to YTH-domain-containing proteins, HNRNP proteins have also been shown to recognize m[6]A[28–30]. Whether additional m[6]A-reader proteins exist is currently unclear. Furthermore, it is currently unknown whether certain proteins are specifically repelled by m[6]A-containing mRNA sequences, a phenomenon that is observed, for example, for methylated DNA[31].

Here we describe global mass-spectrometry-based interaction screening for m[6]A readers in various cell types and mRNA sequence contexts. Our data show that YTH proteins are conserved, cell-type-independent m[6]A readers. In addition, we identified sequence-context-dependent m[6]A readers, including FMR1, thus linking m[6]A to the regulation of mRNA translation and fragile X–linked mental retardation[32]. Strikingly, our data also show that many proteins have a preference for unmodified versus m[6]A- containing mRNA. One such repelled protein is G3BP1, a known stress granule protein[33]. Our RNA-seq and pulsed-SILAC experiments showed that G3BP1 and FMR1 regulate m[6]A-linked mRNA stability and translation rates, respectively. In summary, our data reveal intricate interplay between m[6]A readers and repelled proteins and various aspects of mRNA homeostasis.

RESULTS

The m[6]A interactome in mammalian cells

To identify readers for m[6]A, we carried out RNA pulldowns in mammalian cell lysates followed by quantitative mass-spectrometry-based proteomics (Fig. 1 and Supplementary Fig. 1a). To this end, we designed RNA probes containing four repeats of the m[6]A consensus sequence GGACU[9,10]. As a control, we used an unmethylated strand (Supplementary Fig. 1a). We incubated immobilized probes (Supplementary Fig. 1b–d, Supplementary Table 1) with 'light' (L) and 'heavy' (H) SILAC-labeled lysates. Each

experiment consisted of a 'forward' and a 'reverse' (label-swap) pulldown. After incubation and washes, bound proteins were subjected to on-bead trypsin digestion and analyzed by liquid chromatography–tandem mass spectrometry (LC-MS/MS) (Supplementary Fig. 1a). Supplementary Figure 1a, which depicts a typical RNA-pulldown interaction plot, shows readers in the upper right quadrant (high forward H/L ratio; low H/L ratio in the reverse experiment). Proteins appearing in the lower left quadrant bound preferentially to the unmodified probe. Background proteins are clustered together around the origin of the plot, and showed ~1:1 ratios in both experiments.

We identified 21 m^6A readers in HeLa nuclear (Fig. 1a) and cytoplasmic (Fig. 1b) lysates. YTH-domain-containing proteins were among the most prominent m^6A readers (Fig. 1a,b, Supplementary Data Set 2). We identified ALKBH5, an m^6A demethylase[3], as a reader for m^6A-containing RNA, which indicates that our pulldown approach was able to capture putative enzymes involved in m^6A metabolism. Other prominent m^6A readers are FMR1 and its paralogs FXR1 and FXR2. We also identified three HNRNP proteins as m^6A readers in HeLa nuclear lysates. Other HNRNP proteins—namely, HNRNPG[30], HNRNPC[29] and HNRNPA2B1 (ref. 28)—have previously been linked to m^6A. These proteins recognize m^6A in a structure- and sequence-dependent context, which is probably why they were missing in our pulldowns. An analysis of Gene Ontology (GO)-term enrichment in m^6A readers in HeLa cells showed, as expected, that the most enriched biological pathways among m^6A readers are related to mRNA metabolism and processing (Fig. 1c).

Epigenetic modifications such as m^5C not only recruit but also repel proteins[31]. We identified a number of proteins that preferentially interacted with the unmodified RNA sequence and thus are repelled by m^6A. Prominent among these were two RNA-binding proteins, G3BP1 and G3BP2, both of which are known stress granule proteins[34], as well as their known interaction partners USP10 and CAPRIN1 (ref. 35). This indicates that in our RNA pulldowns we identified both direct RNA-protein interactors and indirect RNA-protein interactors, which are mediated by protein-protein interactions. Another repelled protein is METTL16, which was very recently identified as an adenosine methyltransferase for small nuclear RNA[36]. GO-term enrichment analysis of proteins that are repelled by m^6A revealed terms related to mRNA splicing and transport (Fig. 1d).

Although m^6A levels are mostly stable in different cell types, the m^6A interactome may vary between different cell types. To address this, we carried out m^6A pulldowns in mouse embryonic stem cells (mESCs), neuronal progenitor cells and NIH 3T3 cell lysates. In mESCs, Yth proteins, Alkbh5 and Fmr1 proteins represented the most prominent m^6A readers, which is consistent with data obtained for HeLa cells (Supplementary Fig. 1e,f). G3bp1 and G3bp2, along with Usp10, again represented the most prominent repelled proteins. RNA pulldowns in mouse neuronal progenitor cell lysates combined with a chemical stable-isotope labeling strategy (dimethyl labeling) once again showed that Yth-domain-containing proteins were conserved, cell-type-independent m^6A interactors (Supplementary Fig. 1g,h). m^6A interactors in NIH 3T3 cells were similar to those identified in other cell types. Repelled proteins, however, tended to be more diverse and numerous between different cell types (Supplementary Fig. 1i, Fig. 1e,f).

To discriminate between m^{6}A readers that are dependent on or independent of the RNA sequence context, we generated two different probes with degenerate sequences surrounding m^{6}A and then used these baits for RNA pulldowns in mouse whole cell extracts. From the results, it is clear that YTH-domain-containing proteins largely interacted with m^{6}A in an RNA-sequence-context-independent manner, whereas other readers, such as FMR1, showed RNA-sequence-context-dependent binding. Repelled proteins showed limited overlap between different degenerate strands (Supplementary Fig. 1j,k). A global analysis of RNA-binding domains present among m^{6}A readers and repelled proteins showed that apart from the YTH domain, the KH, RRM and RBD domains were predominant, which indicates that some of these domains may be regulated by m^{6}A directly, albeit in most cases in an RNA-sequence-context-dependent manner (Fig. 1g, Supplementary Fig. 1l).

Finally, we reasoned that certain proteins identified in our screens may have been identified previously in large-scale mRNA interactome studies, which have been conducted via mRNA-protein cross-linking methodologies in HeLa[37], HEK293T[38] and mESC[39] mRNA-protein binding resources (Fig. 1h). A substantial number of the m^{6}A readers that we identified in our pulldowns are also covered in these large-scale mRNA-protein cross-linking studies, which indicates that at least in some cases, these detected *in vivo* mRNA-protein interactions are driven or regulated by mRNA modifications such as m^{6}A.

Stress granule protein G3BP1 is repelled by m^{6}A and regulates mRNA stability

One important observation from our pulldown experiments is that many proteins are repelled by the m^{6}A modification. The two most consistently and strongly repelled proteins were G3BP1 and G3BP2 (G3BPs). These proteins are known to have critical roles in stress granule assembly[33] and are important for embryonic development. G3BPs have very similar domain structures and contain canonical RNA-binding domains[40] (Fig. 2a). First, we used recombinant protein to validate preferential G3BP1 binding to the unmodified RNA. We carried out pulldown experiments in two predominant m^{6}A sequence contexts: GGm^{6}ACU and GAm^{6}ACU[41] (Fig. 2b). In agreement with our quantitative mass spectrometry results (Fig. 1), G3BP1 clearly interacted with the GGACU probe, but not with the GGm^{6}ACU probe. This methylation-sensitive binding was less clear in the GAACU sequence context (Fig. 2b). We further verified these results via quantitative mass spectrometry (Supplementary Fig. 2a). Thus, we conclude that G3BP1 is repelled by m^{6}A in an RNA-sequence-context-dependent manner.

To identify global mRNA binding sites for G3BP1 and G3BP2, we carried out PAR-CLIP (photoactivatable ribonucleoside-enhanced cross-linking and immunoprecipitation) analyses in HEK293T cells with Flag-tagged constructs (Fig. 2c,d, Supplementary Fig. 2b). We identified ~3,800 and ~3,300 mRNA binding sites for G3BP1 and G3BP2, respectively; ~2,300 of these were shared between both proteins (Fig. 2e, Supplementary Data Set 3). At the transcript level, G3BP1 bound to 2,019 genes, whereas G3BP2 bound to 1,672 genes (Fig. 2e); 1,377 target genes were shared between G3BP1 and G3BP2. Most G3BP peaks were found in the 3′-UTR region, followed by intergenic and coding regions (Supplementary Fig. 2c). As has been observed for m^{6}A[10,42], G3BP-binding sites were enriched at 3′-UTR regions (Fig. 2f). However, unlike for m^{6}A, 5′-UTR regions showed

less G3BP binding. The most predominant mRNA-binding motif of G3BP1 was CAACUC ($P = 1 \times 10^{-81}$), whereas CAACUCU was the most predominant binding motif of G3BP2 ($P = 1 \times 10^{-76}$) (Fig. 2g). These motifs were enriched in 31% and 35% of G3BP1 and G3BP2 binding sites, respectively. Thus, the central part of the known m[6]A consensus sequence (ACU) was conserved among G3BP-binding sites. GO-term enrichment analysis showed that G3BP1-bound mRNAs were significantly enriched for intracellular protein trafficking, mRNA splicing and pre-mRNA processing (Fig. 2h), whereas G3BP2-bound mRNAs were enriched for intracellular protein trafficking, chromatin packaging and the cell cycle (Supplementary Fig. 2d). These results indicate that G3BPs regulate mRNAs with both diverse and overlapping biological functions.

Next, we set out to investigate the potential interplay between m[6]A and G3BP1. Approximately 25% of G3BP1 target genes and 23% of G3BP2 target genes are known to carry m[6]A (Fig. 2i). On these target genes, the m[6]A site frequently overlaps with the binding site for G3BP1/G3BP2 (88% and 92%, respectively) (Fig. 2j). This held true in comparisons of G3BP PAR-CLIP data with recently published base-resolution m[6]A data[43] (Fig. 2k). This indicates that at least a fraction of mRNA G3BP1- and G3BP2-binding sites are direct targets for m[6]A. In certain cases—for example, in a GGACU context—m[6]A would inhibit G3BP binding. To further support this observation, we plotted the distance between G3BP peaks relative to previously reported YTHDF2 and YTHDC1 PAR-CLIP data[19,24]. This analysis showed that a substantial amount of G3BP and YTHDF2/YTHDC1 peaks overlap, which further suggests that mRNA binding of G3BPs could be regulated by m[6]A (Supplementary Fig. 2e–h). However, it should once again be noted that many G3BP1-binding sites occur in a sequence context (AACU) in which methylation may not negatively affect G3BP1 binding.

Given that m[6]A negatively correlates with mRNA stability and that G3BP1 binding to mRNA is negatively affected by m[6]A in certain sequence contexts, we reasoned that G3BP1 binding might have a positive effect on the stability of target mRNAs. To address this, we integrated G3BP1 PAR-CLIP data with global mRNA half-life data[44]. First, we assessed the effect of m[6]A on mRNA half-life. As reported previously[19], we observed a negative correlation between mRNA half-life and m[6]A (Fig. 3a). Because YTHDF2 is the main effector of m[6]A-induced mRNA degradation, we also correlated YTHDF2 PAR-CLIP data[19] to mRNA half-life. As was observed for m[6]A, YTHDF2 binding was negatively correlated with mRNA half-life (Fig. 3b). The effect of YTHDF2 binding on mRNA half-life can be completely explained by the amount of m[6]A on the protein's mRNA targets (Supplementary Fig. 3a). Next, we correlated the effect of G3BP1 binding to the half-life of mRNA targets. Here we observed a significant increase in mRNA half-life concordant with an increasing number of G3BP1 binding sites on target mRNAs (Fig. 3c; $P < 2.2 \times 10^{-16}$).

To further investigate the role of G3BP1 in regulating mRNA half-life, we carried out G3BP1 expression perturbation experiments combined with RNA-seq (Fig. 3d–f, Supplementary Data Set 4). We added actinomycin D to cells that contained either reduced or increased amounts of G3BP1 in order to inhibit new mRNA synthesis. Next, we carried out RNA-seq on equal numbers of cells at fixed time points after the addition of actinomycin D. We added an ERCC spike-in to the purified RNA, which, combined with accurate

quantification of cell numbers, facilitated absolute mRNA quantification. As expected, G3BP1 knockdown resulted in a significant decrease in the stability of G3BP1 target mRNAs (Fig. 3g). In agreement with the *in silico* analysis (Fig. 3c), the number of G3BP1 binding sites on target mRNA molecules correlated with the stability of those mRNAs. mRNA targets with one G3BP1-binding site showed decreased stability after G3BP1 knockdown, but this effect was more pronounced for targets that contained more than one binding site. In contrast, after G3BP1 overexpression, we observed a small but consistent increase in the stability of target transcripts (Fig. 3g). We also validated some of these results by qPCR (Supplementary Fig. 3b,c). Together, these results strongly suggest that G3BP1 binding to target mRNAs results in stabilization of the targets.

Finally, to investigate whether the stabilizing effects of G3BP1 binding to target mRNA molecules can be regulated by m^6A, we determined mRNA half-lives after METTL3 knockdown alone or in combination with G3BP1 depletion (Fig. 3h). When m^6A levels were reduced by METTL3 knockdown, we observed a significant increase in the stability of G3BP1 target mRNAs (Fig. 3i). This phenocopied the observed effects of G3BP1 overexpression (Fig. 3g). Combined knockdown of METTL3 and G3BP1 negated this effect (Fig. 3j). We thus conclude that the increased mRNA stability observed after METTL3 knockdown is at least partially caused by increased G3BP1 binding to these transcripts. In summary, these results reveal the intricate interplay among m^6A, m^6A readers, and proteins that are repelled by m^6A to regulate mRNA stability and turnover.

FMR1 interacts with and regulates translation of m^6A-containing transcripts

In both mouse and human cells, we consistently identified FMR1 as an RNA-sequence-context-dependent m^6A reader (Fig. 1, Supplementary Fig. 1). We first set out to verify this observation by using recombinant protein. As shown in Figure 4a,b, recombinant FMR1 preferentially bound to the methylated GGACU RNA probe. As a negative control, we used an FMR1 point mutant (I304N) that is known to be defective in mRNA binding. FMR1 contains two N-terminal Agenet domains, three KH domains and one RGG domain, which are known RNA-binding domains[45]. Very recently, it was shown that under certain conditions RGG domains recognize m^6A-modified RNA[30]. To identify the domain(s) responsible for m^6A binding, we generated several FMR1 GST-deletion constructs (Supplementary Fig. 4a). RNA pulldowns with these deletion constructs showed that all four RNA-binding domains were needed for preferential m^6A binding (Supplementary Fig. 4b). These data thus validate our mass spectrometry data and confirm that FMR1 preferentially interacts with m^6A-containing RNA *in vitro* in certain sequence contexts.

FMR1 binds to hundreds of mRNAs to negatively regulate their translation, and loss of FMR1 leads to fragile X–linked mental retardation syndrome[32,46,47]. Given the overlap between the m^6A and FMR1 consensus mRNA sequences (Fig. 4c)[48] and our *in vitro* interaction data, we asked whether FMR1 preferentially interacts with m^6A-containing mRNA *in vivo*. To address this, we first integrated previously published m^6A-sequencing and FMR1 PAR-CLIP data[10,48]. We observed clear enrichment of mRNA binding by FMR1 isoforms 1 and 7 on m^6A sites, suggesting that FMR1 binding may co-occur with m^6A on mRNA (Fig. 4d). However, the observed spatial proximity between FMR1 and m^6A could

have been due to overlapping FMR1 and m[6]A consensus motifs, rather than (partially) driven by direct m[6]A binding. To determine whether FMR1 preferentially binds to m[6]A-containing mRNA *in vivo*, we carried out cross-linking immunoprecipitation followed by quantitative ultra-high-performance liquid chromatography–tandem mass spectrometry (CLIP-UPLC-MS/MS) to directly measure levels of Flag-FMR1-bound m[6]A. We subjected HEK293T cells with stable expression of Flag-FMR1 to UV cross-linking, after which we carried out immunoprecipitation of FMR1 from whole cell extracts. As negative controls, we carried out Flag pulldowns from Flag and Flag-FMR1-I304N cells (Fig. 4e,f, Supplementary Fig. 4c). Next, we analyzed immunopurified mRNA samples by mass spectrometry to determine the amount of m[6]A in the samples. We observed specific enrichment of m[6]A (more than two-fold) compared with the input in cells that expressed Flag-FMR1 (Fig. 4g). Measurements of m[6]A levels in the immunoprecipitated RNA without RiboMinus treatment did not show any significant differences in m[6]A levels among the three samples (Supplementary Fig. 4d), which indicates that the enriched m[6]A signal was indeed derived from mRNA. Together, these results show that FMR1 colocalizes with m[6]A on mRNA and preferentially interacts with m[6]A-containing mRNA molecules *in vivo*.

Because FMR1 binds to m[6]A and is known to repress translation by stalling ribosome translocation[47], we asked what the biological consequence of FMR1 binding to m[6]A-containing mRNA might be. Recent studies demonstrated a positive correlation between m[6]A and translation mediated by YTHDF1 (ref. 22) and YTHDF3 (ref. 27) in HeLa cells. First, to investigate whether YTHDF1 and FMR1 bind to overlapping mRNA targets, we mined published PAR-CLIP data sets for both proteins in HeLa cells[22,48]. This analysis revealed significant overlap between the two binding profiles, suggesting that a large subset of target mRNAs are shared ($P < 1.259 \times 10^{-38}$; Fig. 4h). We even observed significant overlap between FMR1 targets in mouse brain[47] and YTHDF1 targets in HeLa cells ($P < 7.120 \times 10^{-112}$) (Supplementary Fig. 4e), which indicated that many of the overlapping targets are cell-type independent. Common targets included HUWE1 and KDM5C, which are also implicated in X-linked mental retardation disorders. GO-term enrichment analysis of common FMR1/YTHDF1 target genes between brain and HeLa cells highlighted biological processes related to neurogenesis (Supplementary Fig. 4f).

To investigate the potential interplay among FMR1, m[6]A and translation rates, we made use of a pulsed-SILAC-based method[49] (Fig. 4i, Supplementary Data Set 5). Briefly, we grew HeLa cells that expressed either inducible FMR1 or FMR1-I304N in light (Lys0Arg0 (K0R0)) medium. We induced transgene expression for 24 h (Fig. 4j), after which we transferred the induced cells to medium-heavy (M) (K4R6) SILAC medium, whereas we transferred non-induced control cells to heavy (K8R10) SILAC medium. We harvested different batches of cells at 2, 6, 10 and 24 h after transfer to medium-heavy or heavy SILAC medium. The incorporation of SILAC labels during this incubation provided a proxy for the translation rates. Furthermore, comparison of the M/L and H/L ratio for each protein provided a readout for the effect of transgene expression on translation rates (Fig. 4k). The translation rate was defined as the time needed for half of each quantified protein to be labeled with the given SILAC label[50]. At the global level, FMR1 expression resulted in global translational inhibition compared with the expression of FMR1-I304N (Fig. 4l). To investigate the potential interplay between the regulation of translation by FMR1 and m[6]A,

we carried out a second pulsed-SILAC experiment in which we combined FMR1 or FMR1-I304N expression with simultaneous METTL3 knockdown (Fig. 4j). As expected, a reduction of m[6]A levels in cells expressing the FMR1-I304N mutant led to decreased translation rates (Fig. 4l). Notably, the negative effect of wild-type FMR1 expression on translation was aggravated by a simultaneous reduction in the amount of m[6]A (Fig. 4l, Supplementary Fig. 4g). We interpret this as follows: YTH-domain-containing proteins are strictly dependent on m[6]A for mRNA binding. Their positive effects on translation are therefore mitigated by METTL3 knockdown and the concomitant reduction of m[6]A levels. FMR1 preferentially binds m[6]A-containing mRNA, but it is not strictly dependent on m[6]A for mRNA binding (Fig. 4a). On the basis of our results, we propose that YTHDF1 and FMR1 compete for binding to m[6]A sites on mRNA. Thus, after METTL3 knockdown, the inhibitory effects of FMR1 on translation rates become even more pronounced, because many putative ACU-containing FMR1-binding sites become available in the absence of YTHDF1/3. These results further illustrate the complex interplay among m[6]A, m[6]A readers and mRNA homeostasis.

DISCUSSION

Here we describe a systematic mass-spectrometry-based proteomics screen to identify m[6]A readers in a variety of cell types and different RNA sequence contexts. Our data show that YTH-domain-containing proteins are evolutionarily conserved cell-type-independent m[6]A readers. In addition, we identified a number of previously unrecognized m[6]A readers, although we emphasize that almost all of these newly identified readers, including FMR1, interact with m[6]A in a manner that is dependent on RNA sequence, and possibly also the secondary structure context. Multiple RNA-binding domains may be responsible for these RNA-sequence-dependent m[6]A interactions, such as the KH and RGG domains. Additional biochemical studies are clearly needed to further investigate this. These observations are analogous to what has been observed for DNA-methylation readers. DNA methylation is read by a few DNA-sequence-independent domains[31]. In addition, other domains, such as the Forkhead box, Krueppel-like zinc fingers and the homeobox, interact with methylated DNA sequences in a DNA-sequence-dependent manner.

One important conclusion from our work is that m[6]A could serve to repel proteins from binding to m[6]A-containing mRNA sequences. This is again analogous to what has been observed in the context of DNA methylation[31]. For RNA sequences that contained ACU motifs, we observed a lot of interacting proteins, and for a substantial number of those, binding was inhibited when the adenosine base in the sequence was methylated. The most strongly repelled proteins in our RNA pulldown experiments were G3BP1 and G3BP2. However, this phenomenon seems to be dependent on the RNA sequence context. In a GGACU context, m[6]A strongly repelled G3BP1 binding, whereas inhibition of binding was not obvious when methylation occurred in a GAACU context (Fig. 2b). The results of our functional experiments for G3BP1 (Figs. 2 and 3) suggest that G3BP1 binding to mRNA is positively correlated with mRNA stability, and that this positive correlation can be affected by manipulation of m[6]A levels. mRNA stability in *cis* is mediated by three major factors: (1) the extent of m[6]A presence, (2) polyadenylation and (3) codon optimization[51]. Of these three factors, m[6]A is the only one that can be dynamically altered through methylation and

demethylation. The *cis* factors are aided by *trans* factors such as protein readers, which regulate the stability of mRNA. It was previously reported[19] that YTHDF2 predisposes mRNA to degradation in an m^6A-dependent manner. Our data suggest that G3BP1 is one additional m^6A-regulated factor that affects RNA stability. G3BP1 could stabilize mRNA molecules in several ways. G3BP1 is found in the nucleus in resting cells[52], and it could bind to newly transcribed mRNA molecules in the nucleus and prevent methylation by competing with the m^6A methylation machinery. Alternatively, G3BP1 could bind to its target mRNAs in the cytoplasm and form ribonucleoprotein granules (RNPs). These RNPs could assemble into higher-order stress granules consisting of other proteins and translation factors[53]. The formation of G3BP1-mRNA RNPs or stress granules could prevent access to the RNA degradation machinery, thereby protecting mRNA. Another possible mechanism is that under certain conditions, cells could demethylate mRNA, thereby allowing G3BP1 to bind to GGACU-containing mRNA sequences, resulting in increased stability of those mRNA molecules. Interestingly, G3BP1 is also known to bind inosine[54], a modified adenosine base, which indicates a broader role for G3BPs in RNA-modification-dependent modulation of mRNA homeostasis. In any case, our findings reveal intricate interplay between RNA-binding proteins and the regulation of mRNA homeostasis. Dynamic m^6A levels in cells, which affect many RNA-binding proteins, seem to represent a regulatory switch via which mRNA stability and translation can be quickly fine-tuned to regulate gene expression and cell function in the presence of cellular stimuli and perturbations.

The work presented here is also relevant from a clinical perspective. It is well established that m^6A has an important role in the regulation of mRNA homeostasis. It is therefore not surprising that disturbances of readers, writers and erasers of m^6A are implicated in a number of diseases, including obesity and cancer[14,15]. We have identified FMR1, an important constituent of neuronal granules and stress granules[55], as a clinically relevant, RNA-sequence-context-dependent reader for m^6A. FMR1 binds to ribosomes and represses the translation of target mRNAs. Loss of this repression in neurons due to the absence of functional FMR1 leads to fragile X–linked mental retardation[47]. Our work suggests that a reduction of m^6A levels or inhibition of YTHDF1, both of which inhibit mRNA translation, may result in the alleviation of disease symptoms in fragile X–linked mental retardation syndrome. Further work, however, is clearly needed to test this hypothesis. In any case, our work here has uncovered what is, to the best of our knowledge, the first reported link between an mRNA modification and an autism spectrum disorder, thus paving the way toward a better molecular understanding, and possibly treatment, of this disease.

ONLINE METHODS

Cell culture, SILAC labeling and cell-extract preparation

HeLa, HEK293T and NIH 3T3 cells were cultured in Dulbecco's modified Eagle's medium (DMEM; Thermo) supplemented with 10% FBS (Gibco), 1× penicillin–streptomycin (15140-122; Thermo) and 1 mM glutamine (Invitrogen). The cells were regularly tested in-house for the presence of mycoplasma. HeLa cells were SILAC-labeled by culture in SILAC DMEM (88420; Thermo) supplemented with 10% dialyzed FBS (DS-1003; Dundeecell), 1× Glutamax (35050-061; Thermo), 1× penicillin– streptomycin, 73 mg/mL -lysine (light/K0,

Sigma, A6969; or heavy/K8, Sigma, 608041) and 29.4 mg/mL arginine (light/R0, Sigma, A6969; or heavy/R10, Sigma, 608033). ESCs were grown in serum-free 2i medium. Briefly, we prepared serum-free ESC medium by mixing the following components: Neurobasal medium (Gibco; 21103-049), 250 mL; DMEM/F12 (Gibco; 11320-033), 250 mL; N2-Supplement (Gibco; 17502-048), 2.5 mL; B27 minus RA (Gibco; 12587001), 5 mL; 7.5% BSA (Gibco,;15260-037), 3.33 mL; penicillin–streptomycin, 5 mL; 1 mM glutamine (Invitrogen); 1% nonessential amino acids (Invitrogen); 6.3 μl monothioglycerol (M6145; Sigma); LIF (1,000 U/mL); and CHIR99021 and PD0325901 (3 and 1 μM, respectively). For SILAC labeling of ESCs, we used custom-made Neurobasal and DMEM/F12 (Life technologies) without lysine and arginine. Mouse neuronal progenitor cells were cultured as described previously[56].

Whole cell lysates for RNA pulldowns were prepared according to the following protocol: Cells were harvested with trypsin and washed twice with chilled PBS. Cells were then resuspended in five pellet volumes of whole cell extract buffer (50 mM Tris-HCl, pH 8, 150 mM NaCl, 1% NP-40, 0.5 mM DTT, 10% glycerol, and protease inhibitor cocktail) and incubated for 90 min at 4 °C on a rotating wheel. Crude lysates were then centrifuged for 30 min at 14,000 r.p.m. at 4 °C. Soluble whole cell extracts were finally aliquoted and snap-frozen in liquid nitrogen until further usage. Nuclear and cytoplasmic extracts were prepared as described previously[56]. Cell lysates for western blots were prepared with RIPA buffer (10 mM Tris-Cl, pH 8.0, 1 mM EDTA, 1% Triton X-100, 0.1% sodium deoxycholate, 150 mM NaCl, 0.1% SDS and protease inhibitor cocktail). Protein quantification was performed with a Bradford or BCA kit (Thermo) according to the manufacturer's protocol.

Plasmids and constructs

G3BP1 cDNA was cloned into the *Hin*dIII and *Bam*HI sites of pcDNA3-c-Flag vector (Plasmid #20011; Addgene) to create an expression construct with a C-terminal Flag tag. For the creation of N-terminally GST-tagged constructs, G3BP1 cDNA was amplified from HeLa cDNA and cloned into pGEX-5X1 vector (GE Healthcare). FMR1 isoform 1 (pFRT-TODestFLAGHAhFMRPiso1; 48690) and FMR1-I304N isoform 1 (pFRT-TODestFLAGHAhFMRPiso1I304N; 48692) vectors were obtained from Addgene. FMR1, FMR1-I304N and various domains of FMR1 were amplified from these vectors. We created FMR1 overexpression constructs for the creation of doxycycline-inducible HeLa cell lines by subcloning FMR1 and FMR1-I304N in AAVS1-TRE3G-EGFP (Addgene; 52343). A Kozac sequence and a Flag-HA tag were added to the N terminus of FMR1 and FMR1-I304N by PCR. AAVS1-TRE3G-EGFP[57] contains an inducible promoter and AAVS1 homology arms for correct integration. By cloning FMR1 in *Sal*I and *Mlu*I sites, we generated an AAVS1-TRE3G-FMR1 construct. Primer sequences used to amplify specific genes and constructs are listed in Supplementary Table 1.

Generation of cell lines

We generated HeLa cells expressing inducible FMR1 and FMR1-I304N by knocking Flag-HA-FMR1 or the I304N mutant into the AAVS1 locus. To this end, HeLa cells were transfected with a donor vector (AAVS1-TRE3G-FMR1) and a CRISPR-Cas9 vector with guide RNAs targeting the AAVS1 locus[58], using Lipofectamine 3000 (Invitrogen). In this

system, cells with correct integration at the AAVS1 locus become puromycin resistant. Cells with stably integrated gene products were selected by puromycin (1 μg/mL) selection for several days. Individual colonies were picked, and doxycycline-induced expression was tested for several clones. Overexpression of FMR1 and FMR1-I304N was induced by the addition of 1 and 0.5 μg/mL doxycycline, respectively.

Recombinant protein expression and purification

Rosetta BL-21 bacteria (Novagen) were used for GST-fusion protein expression. Cells were grown in LB medium supplemented with 100 μg/mL ampicillin and 34 μg/mL chlo-ramphenicol. IPTG was added to a final concentration of 0.5 mM, after which protein expression was induced for 4 h or overnight at 16 °C. Cells were then harvested, washed with PBS and resuspended in lysis buffer (50 mM Tris-HCl, pH 8.0, 15% glycerol, 1 mM EDTA, 0.5 mM PMSF, 1 mM DTT, 100 mM NaCl, 1% Triton X-100, 0.25% NP-40, protease inhibitor cocktail, and lysozyme to a final concentration of 0.5 mg/ml). Cells were lysed by repeated (five times) freeze-thaw cycles. Bacterial debris was removed by centrifugation at 14,000 r.p.m. for 20 min at 4 °C, after which soluble extracts were aliquoted and snap-frozen in liquid nitrogen until further usage.

SILAC-based RNA pulldowns

All buffer solutions were prepared with high-quality, RNase-free reagents. Each SILAC-based RNA pulldown experiment consisted of four individual pulldowns. 10 μl of streptavidin Sepharose high-performance beads (GE Healthcare) were used for each pulldown (20 μl of 50% slurry). Beads were first washed twice in 1 mL of RNA binding buffer (50 mM HEPES-HCl, pH 7.5, 150 mM NaCl, 0.5% NP40 (v/v), 10 mM $MgCl_2$). After each wash step, samples were centrifuged for 3 min at 4,000 r.p.m. in a pre-cooled (4 °C) tabletop centrifuge to spin down the beads. To inactivate and remove RNases, we incubated the beads with RNase inhibitor RNasin plus (Promega) in RNA binding buffer (100 μl buffer with 0.8 units of RNasin/μl) for 30 min on ice. After centrifugation and removal of RNasin–RNase complexes, beads were preblocked with yeast tRNA (50 μg/mL; AM7119; Life Technologies) in RNA binding buffer overnight at 4 °C on a rotation wheel. The preblocked beads were washed twice with RNA binding buffer and then incubated with 5 μg of bioti-nylated RNA probe (per pulldown) diluted with RNA binding buffer to a final volume of 600 μl. Beads were incubated for 30 min at 4 °C in a rotation wheel to allow binding of biotinylated probes to the streptavidin beads. The beads were washed once with 1 mL of RNA wash buffer (50 mM HEPES-HCl, pH 7.5, 250 mM NaCl, 0.5% NP-40 and 10 mM $MgCl_2$) and twice with protein incubation buffer (10 mM Tris-HCl, pH 7.5, 150 mM KCl, 1.5 mM $MgCl_2$, 0.1% (v/v) NP-40, 0.5 mM DTT, and complete protease inhibitors −/− EDTA (Roche)). Beads containing immobilized RNA were then incubated with 600 μg of nuclear extract or 1,000 μg of cytoplasmic extracts in a total volume of 600 μl of protein binding buffer. The incubation reaction also contained 30 μg of yeast tRNA to prevent nonspecific binding, and RNasin. In the forward experiment, the control probe was incubated with light-labeled (R0K0) lysates, whereas the m6A probe was incubated with heavy (R10K8) lysates. The reverse experiment represented a biological-replicate label swap. The reactions were incubated at room temperature for 30 min and then for 90 min on a rotation wheel at 4 °C. The beads were then washed three times with protein incubation

buffer and twice with ice-cold PBS to remove detergent from the beads. The last PBS wash was used to combine beads from the forward and the reverse pulldowns as follows:

Forward reaction: control probe, R0K0 (light); m^{6}A probe, R10K8 (heavy)

Reverse reaction: control probe, R10K8 (heavy); m^{6}A probe, R0K0 (light)

Proteins were on-bead digested with trypsin. Briefly, beads were resuspended in 100 μL of elution buffer (50 mM Tris, pH 8.5, 2 M urea and 10 mM DTT) and then incubated for 20 min at room temperature in a thermoshaker at 1,100 r.p.m. Iodoacetamide was then added to a final concentration of 55 mM, and the mixture was incubated for 10 min in a thermoshaker (1,100 r.p.m.) at room temperature in the dark. Proteins were then partially digested from the beads by the addition of 250 ng of trypsin for 2 h at room temperature in a thermoshaker in the dark. After incubation, the supernatant was collected in a separate tube. The beads were then incubated with 50 μL of elution buffer for 5 min at room temperature in a thermoshaker (1,100 r.p.m.). 100 ng of fresh trypsin was added to the pooled eluates, and proteins were digested overnight at room temperature. Finally, tryptic peptides were acidified to pH <2 with TFA (10%) and desalted with C18 Stage tips before MS analyses.

Dimethyl-labeling-based RNA pulldowns

Dimethyl-labeling-based RNA pull-downs were performed with unlabeled lysates. Tryptic peptides from individual pulldowns obtained after on-bead digestion were differentially labeled with dimethyl isotopes (CH_2O or CD_2O) essentially as described[59]. We created forward and reverse reactions by mixing labeled peptides as follows:

Forward reaction: control probe, CH_2O (light); m6A probe, CD_2O (medium)

Reverse reaction: control probe, CD_2O (medium); m6A probe, CH_2O (light)

Labeled reactions were acidified to pH <2 with TFA (10%) and desalted with C18 Stage tips before MS analyses. RNA probes used in SILAC and dimethyl-labeling-based pulldowns are listed in Supplementary Table 1.

siRNA knockdown

siRNAs targeting human G3BP1 (SR306845) or METTL3 (SR311159) and control siRNAs (SR30004) were obtained from Origene. siRNAs were transfected at a final concentration of 25 nM using Lipofectamine 3000 (Invitrogen) according to the manufacturer's instructions.

Quantitative RT-PCR

qRT-PCR reactions were done with iQ SYBR Green Supermix. Oligonucleotides used in this study are listed in Supplementary Table 1.

Western blot analyses and antibodies

SDS-PAGE gels were blotted onto nitrocellulose membrane with the Trans-Blot Turbo transfer system (Bio-Rad). Blots were stained with Ponceau stain to confirm equal loading of proteins. Blots were blocked in 5% skim milk in PBS. Primary antibodies to the following proteins were used: G3BP1 (Santa Cruz Biotechnology; sc-98561), Flag (Sigma-Aldrich;

F1804), GST (Thermo; MA4-004) and METTL3 (Bethyl Laboratories; A301-567-A). Images were processed in ImageJ. Western blot quantifications were done with ImageJ.

FMR1 CLIP

2.4×10^8 HEK293T cells stably expressing Flag-HA, Flag-HA-FMR1, or Flag-HA-FMR1-I304N were UV-cross-linked twice with 150 mJ/cm^2 at 254 nm and harvested with a cell scraper. Cells were lysed in two volumes of lysis buffer containing 150 mM KCl, 2 mM EDTA, 10 mM HEPES, 0.5% NP-40, 0.5 mM DTT, 1:100 cOmplete protease inhibitor (Roche; 04693116001), and 1:100 SUPERase In RNase inhibitor (20 U/μL; Ambion; AM2694) for 30 min in a rotation wheel at 4 °C. Lysate was cleared by centrifugation at 14,000 r.p.m. for 15 min at 4 °C followed by syringe filtration through a 0.45-μm filter. 50 μL of lysate was saved as input. 200 μL of anti-Flag magnetic beads (Sigma; M8823) were washed with 500 μL of ice-cold wash buffer four times (200 mM NaCl, 2 mM EDTA, 0.05% NP-40, 50 mM Tris-HCl, pH 7.6, 0.5 mM DTT, 1:1,000 SUPERase In RNase inhibitor, 1:1,000 protease inhibitor). Lysate was added to the beads and incubated for 2 h on a rotation wheel at 4 °C. Supernatant was removed and saved as flow-through, and beads were washed six times with 1 mL of ice-cold wash buffer. 250 μL of elution solution (500 ng μl^{-1} 3× Flag peptide (Sigma; F4799) in wash buffer) was added to each sample, and the mixture was rotated for 1 h at 4 °C to elute. We made proteinase K solution by adding 10% proteinase K solution (20 mg/mL; Invitrogen; 25530049) to 2× proteinase K buffer (100 mM Tris, pH 7.7, 150 mM NaCl, 12.5 mM EDTA, 2% (w/v) SDS). The eluent, 50 μl of input, and 50 μl of flow-through were each incubated in one volume of proteinase K solution for 45 min at 55 °C to release RNA. Three volumes of TRIzol were added to each sample, and total RNA was extracted on a Direct-zol microprep spin column according to the manufacturer's protocol for RNA extraction and DNase I digestion. rRNA was removed with the RiboMinus Eukaryote Kit v2. 50 ng of input, flow-through, and immunoprecipitated mRNA were analyzed by LC-MS/MS as previously reported[19].

PAR-CLIP

PAR-CLIP was performed as previously reported[19]. Briefly, five 15-cm plates of HEK293T cells were seeded on day 1. After 18 h, the cells were transfected with Flag-tagged G3BP1 or G3BP2 plasmid at 80% confluency. After another 6 h, the media was changed and 200 μM 4SU was added. After 14 h, the media was aspirated and the cells were washed twice with PBS for each plate. The plates were kept on ice, and cross-linking was carried out with 0.15 J/cm^2 365-nm UV light. 2 ml of PBS was added, and the cells were collected with a cell lifter. RNA was purified as previously reported[19]. The purified bound RNA was dissolved in 12 μl of RNase-free water, of which 6 μl was subjected to small RNA library preparation with the NEBNext Multiplex Small RNA Library Prep Set for Illumina (E7300S; NEB). Two biological replicates were carried out for G3BP1 and G3BP2 each. All samples were sequenced on an Illumina HiSeq 2000 with single-end 50-bp read length. For data analysis, the adaptors were trimmed with the FASTX-Toolkit[60]. Deep-sequencing data were mapped to human genome version hg38 with TopHat version 2.0 (ref. 61), without any gaps and allowing for at most two mismatches. PAR-CLIP data were analyzed by PARalyzerv1.1 with default settings[62]. HOMER[63] was used for *de novo* motif discovery. For the comparison of PAR-CLIP and m^{6}A peaks from Liu *et al.*[5] (Fig. 2i,j), at least 1-bp

overlap was applied as the criterion for defining overlapping peaks. To assess the distribution of m6A with respect to PAR-CLIP peaks, we used publicly available single-nucleotide-resolution m6A data from Linder et al.[43] and converted the reported m6A sites to hg38 with liftOver[64]. For FMR1 and m6A colocalization analysis (Fig. 4d), we generated random peaks by randomly permuting the location of m6A peaks on the transcriptome.

GO analysis

GO-term enrichment analysis was performed with DAVID[65]. The top 10–15 most enriched GO terms with a Bonferroni or Benjamini–Hochberg corrected P value of <0.05 were used. To reduce redundancy in the GO terms involved and summarize them, we used the online tool REVIGO[66]. We used Cytoscape[67] to make figures from REVIGO output.

RNA half-life determination

RNA half-life was determined by RNA-sequencing as described previously[19]. Briefly, six 10-cm plates were seeded with HeLa cells at 25% confluency. After 8 h, two plates were transfected with siControl, two with siG3BP1, and two with siG3BP1 + siMETTl3. For overexpression experiments, a Flag-control plasmid and a Flag-G3BP1 construct were transfected into two 10-cm plates of HeLa cells each. 24 h after transfection, cells were trypsinized and live cells were counted. Cells were then equally divided over three fresh plates. 48 h after transfection, actinomycin D was added to a final concentration of 5 μg/mL (Santa Cruz Biotechnology; sc-200906). Cells were then harvested 0, 3 and 6 h after the addition of actinomycin D, respectively. The harvested cells were counted once again and snap-frozen. RNA was purified with the Qiagen RNeasy mini kit. rRNA was removed with the Ribo-Zero rRNA removal kit (Illumina). RNA fragmentation was performed with the NEBNext Magnesium RNA Fragmentation Module (NEB). The first cDNA strand was synthesized with Superscript III in the presence of actinomycin D and random hexamers. The second strand was synthesized with *Escherichia coli* DNA polymerase in the presence of dUTP. USER enzyme was added before library amplification to maintain strand identity. NEXTflex 8-bp adaptors were used for adaptor ligation. Size selection was performed with E-gel, and quality was assessed on a Bioanalyzer.

RNA-seq libraries were quantified with kallisto version 0.43.0 (ref. 68) by pseudo-alignment to the RefSeq transcript database downloaded 28 June 2016. Absolute transcript concentrations per cell were computed by linear-fitting the RNA spike-in TPM values to attomoles. RNA half-life measures were calculated as described by Wang et al.[19]. In short, for every transcript, the RNA-degradation constant was determined as the $\log_2$ fold change in RNA abundance 3 or 6 h after transcription was inhibited, and the average degradation constant was used to calculate the RNA half-life per transcript. To ensure accurate RNA half-life estimations, we considered only transcripts with finite RNA half-lives of <24 h for further analyses. The RNA half-life measures in Figure 3a–c were taken from Tani et al.[44].

Mass spectrometry

Tryptic peptides were separated with an Easy-nLC 1000 (Thermo) connected online to a Q Exactive or Orbitrap-Fusion mass spectrometer (Thermo). RNA pulldown samples were separated with a 94-min acetonitrile gradient (7% to 32%) followed by washes at 50% and

then 95% acetonitrile for a total of 120 min of data acquisition. For measurements on the Q Exactive, the top ten most abundant peptides were fragmented for every full scan. For RNA pulldowns measured on the LTQ-Orbitrap Fusion Tribrid mass spectrometer (Thermo), a similar LC gradient was used, and samples were measured in top-speed mode. For the whole-cell proteome experiment measured on the LTQ-Orbitrap Fusion Tribrid mass spectrometer (Thermo), peptides were separated with a 214-min acetonitrile gradient (7% to 30%) followed by washes at 60% and then 95% acetonitrile for a total of 240 min of data acquisition. Scans were collected in data-dependent top-speed mode in cycles of 3 s with dynamic exclusion enabled and set to 60 s.

MaxQuant analysis

Data processing was done with the MaxQuant software. For SILAC-labeling-based experiments, raw data were analyzed with MaxQuant version 1.5.0.1 with the default settings and K0R0, K4R6 or K8R10 (light, medium-heavy or heavy) labels, and matching between runs enabled[69]. For dimethyl-labeling-based experiments, raw data were analyzed with DimethylLys0 and DimethylLys4 (light and medium) labels, and matching between runs was enabled. We used the UniProt database downloaded on 13 July 2014 for identification. To identify significant interactors, we plotted normalized ratios from MaxQuant output tables for the forward and reverse pulldowns. Outliers were identified independently in the forward and reverse pulldowns by means of box plot statistics (threshold: 1.5× the interquartile range). Proteins were considered significant if they were identified as outliers in both experiments. Proteins identified in MaxQuant output tables were classified into four groups: readers, repelled proteins, background proteins, and contaminants. For whole-cell proteome experiments, we used a Swiss-Prot curated database for identification (downloaded on 7 February 2016). Scatter plots were generated in R.

Pulsed SILAC

Pulsed SILAC is a variant SILAC method used to measure translation rates in cells[49]. HeLa cells expressing FMR1 under doxycycline control were SILAC-labeled in light medium (K0R0) for a week to allow them to adapt to the culture conditions. Doxycycline was added for 24 h to induce expression of FMR1 or the FMR1 mutant. Cells without doxycycline induction served as a control. In the case of FMR1 overexpression combined with METTL3 knockdown, METTL3 siRNAs were transfected 24 h before the addition of doxycycline. Control siRNA was transfected into control cells that were not treated with doxycycline. 24 h after doxycycline induction, cells were washed with PBS to remove any light amino acid–containing medium. Cells with FMR1 overexpression alone or in combination with with METTL3 knockdown were transferred to medium-heavy (K4R6) medium. Non-doxycycline-treated control cells were transferred to heavy (K8R10) medium. Cells were subsequently harvested 2, 6, 10 and 24 h after transfer into medium-heavy or heavy SILAC medium. The harvested cells were then lysed on ice by the addition of 150 μl of lysis buffer (100 mM Tris-HCl, pH 7.6, 4% SDS) and heated for 5 min at 95 °C. The samples were sonicated with a Diagenode Bioruptor to reduce viscosity. Crude lysates were then centrifuged at 14,000 r.p.m. for 20 min, and supernatants were recovered. Lysate protein concentrations were measured with the BCA kit (Thermo). Equal amounts of protein from control and treated samples at each time point were then mixed. DTT was added to a 100

mM final concentration, and the samples were incubated for 15 min. Samples were then further processed via the FASP method[70]. A trypsin-LysC mix (Promega) was used for digestion. Finally, tryptic peptides were acidified to pH <2 with TFA (10%) and desalted with C18 Stage tips before MS analyses.

The time it took for half the protein to be labeled (THPL) was calculated for all identified proteins as described by Visscher *et al.*[50]. In short, we performed a linear regression between the log-transformed fraction of labeled protein and the pulse time. We then extrapolated the THPL by dividing the slope of the regression by log(0.5). In addition to the four pulsed time points, we forced the regression lines though zero as described previously[50]. To ensure high confidence of our individual THPL measurements, we used only the proteins with an identified label ratio in all time points and a Pearson correlation coefficient of 0.95 or higher for downstream analyses.

Statistical analysis

Various statistical methods were used as appropriate and are indicated in the figure legends. The interquartile range (1.5×) was used to identify outliers in affinity-purification mass spectrometry experiments. The *P* values of the identified RBP motifs were determined by HOMER[63]. Significantly enriched gene ontologies were identified with a modified Fisher exact test, after multiple testing correction by the Bonferroni or Benjamini–Hochberg method. A Fisher exact test was used to analyze overlap between PAR-CLIP peaks. Two-sided nonparametric Mann–Whitney *U* tests were used to test for differences in protein half-lives and in mRNA half-lives.

A **Life Sciences Reporting Summary** for this article is available.

Data availability

All mass spectrometric data generated in this study have been deposited to the ProteomeXchange Consortium via the PRIDE repository under project identifier PXD006498. RNA-sequencing and PAR-CLIP data have been deposited at Gene Expression Omnibus (GEO) under accession code GSE98856. Uncropped images of western blots, agarose gels and PAR-CLIP images are in Supplementary Data Set 1. Source data for Figures 1g,h, 2i,j and 4g are available online. Any other data are available from the corresponding author upon request.

Supplementary Material

Refer to Web version on PubMed Central for supplementary material.

Acknowledgments

References

1. Dimock K, Stoltzfus CM. Sequence specificity of internal methylation in B77 avian sarcoma virus RNA subunits. Biochemistry. 1977; 16:471–478. [PubMed: 189800]

2. Desrosiers RC, Friderici KH, Rottman FM. Characterization of Novikoff hepatoma mRNA methylation and heterogeneity in the methylated 5′ terminus. Biochemistry. 1975; 14:4367–4374. [PubMed: 169893]

3. Zheng G, et al. ALKBH5 is a mammalian RNA demethylase that impacts RNA metabolism and mouse fertility. Mol Cell. 2013; 49:18–29. [PubMed: 23177736]

4. Jia G, et al. N^6-methyladenosine in nuclear RNA is a major substrate of the obesity-associated FTO. Nat Chem Biol. 2011; 7:885–887. [PubMed: 22002720]

5. Liu J, et al. A METTL3-METTL14 complex mediates mammalian nuclear RNA N^6-adenosine methylation. Nat Chem Biol. 2014; 10:93–95. [PubMed: 24316715]

6. Ping XL, et al. Mammalian WTAP is a regulatory subunit of the RNA N^6-methyladenosine methyltransferase. Cell Res. 2014; 24:177–189. [PubMed: 24407421]

7. Schwartz S, et al. Perturbation of m^{6}A writers reveals two distinct classes of mRNA methylation at internal and 5′ sites. Cell Rep. 2014; 8:284–296. [PubMed: 24981863]

8. Aguilo F, et al. Coordination of m^{6}A mRNA methylation and gene transcription by ZFP217 regulates pluripotency and reprogramming. Cell Stem Cell. 2015; 17:689–704. [PubMed: 26526723]

9. Dominissini D, et al. Topology of the human and mouse m^{6}A RNA methylomes revealed by m^{6}A-seq. Nature. 2012; 485:201–206. [PubMed: 22575960]

10. Meyer KD, et al. Comprehensive analysis of mRNA methylation reveals enrichment in 3′ UTRs and near stop codons. Cell. 2012; 149:1635–1646. [PubMed: 22608085]

11. Zhao X, et al. FTO-dependent demethylation of N^6-methyladenosine regulates mRNA splicing and is required for adipogenesis. Cell Res. 2014; 24:1403–1419. [PubMed: 25412662]

12. Zhong S, et al. MTA is an *Arabidopsis* messenger RNA adenosine methylase and interacts with a homolog of a sex-specific splicing factor. Plant Cell. 2008; 20:1278–1288. [PubMed: 18505803]

13. Agarwala SD, Blitzblau HG, Hochwagen A, Fink GR. RNA methylation by the MIS complex regulates a cell fate decision in yeast. PLoS Genet. 2012; 8:e1002732. [PubMed: 22685417]

14. Lin S, Choe J, Du P, Triboulet R, Gregory RI. The m^{6}A methyltransferase METTL3 promotes translation in human cancer cells. Mol Cell. 2016; 62:335–345. [PubMed: 27117702]

15. Li Z, et al. FTO plays an oncogenic role in acute myeloid leukemia as a N^6-methyladenosine RNA demethylase. Cancer Cell. 2017; 31:127–141. [PubMed: 28017614]

16. Batista PJ, et al. m^{6}A RNA modification controls cell fate transition in mammalian embryonic stem cells. Cell Stem Cell. 2014; 15:707–719. [PubMed: 25456834]

17. Zhao BS, et al. m^{6}A-dependent maternal mRNA clearance facilitates zebrafish maternal-to-zygotic transition. Nature. 2017; 542:475–478. [PubMed: 28192787]

18. Geula S, et al. m^{6}A mRNA methylation facilitates resolution of naïve pluripotency toward differentiation. Science. 2015; 347:1002–1006. [PubMed: 25569111]

19. Wang X, et al. N^6-methyladenosine-dependent regulation of messenger RNA stability. Nature. 2014; 505:117–120. [PubMed: 24284625]

20. Meyer KD, et al. 5′ UTR m^{6}A promotes cap-independent translation. Cell. 2015; 163:999–1010. [PubMed: 26593424]

21. Zhou J, et al. Dynamic m^{6}A mRNA methylation directs translational control of heat shock response. Nature. 2015; 526:591–594. [PubMed: 26458103]

22. Wang X, et al. N^6-methyladenosine modulates messenger RNA translation efficiency. Cell. 2015; 161:1388–1399. [PubMed: 26046440]

23. Alarcón CR, Lee H, Goodarzi H, Halberg N, Tavazoie SF. N^6-methyladenosine marks primary microRNAs for processing. Nature. 2015; 519:482–485. [PubMed: 25799998]

24. Xiao W, et al. Nuclear m^{6}A reader YTHDC1 regulates mRNA splicing. Mol Cell. 2016; 61:507–519. [PubMed: 26876937]

25. Patil DP, et al. m^{6}A RNA methylation promotes XIST-mediated transcriptional repression. Nature. 2016; 537:369–373. [PubMed: 27602518]

26. Cao G, Li HB, Yin Z, Flavell RA. Recent advances in dynamic m^{6}A RNA modification. Open Biol. 2016; 6:160003. [PubMed: 27249342]

27. Shi H, et al. YTHDF3 facilitates translation and decay of N^6-methyladenosine-modified RNA. Cell Res. 2017; 27:315–328. [PubMed: 28106072]

28. Alarcón CR, et al. HNRNPA2B1 is a mediator of m^{6}A-dependent nuclear RNA processing events. Cell. 2015; 162:1299–1308. [PubMed: 26321680]

29. Liu N, et al. N^6-methyladenosine-dependent RNA structural switches regulate RNA-protein interactions. Nature. 2015; 518:560–564. [PubMed: 25719671]

30. Liu N, et al. N^6-methyladenosine alters RNA structure to regulate binding of a low-complexity protein. Nucleic Acids Res. 2017; 45:6051–6063. [PubMed: 28334903]

31. Spruijt CG, Vermeulen M. DNA methylation: old dog, new tricks? Nat Struct Mol Biol. 2014; 21:949–954. [PubMed: 25372310]

32. Penagarikano O, Mulle JG, Warren ST. The pathophysiology of fragile X syndrome. Annu Rev Genomics Hum Genet. 2007; 8:109–129. [PubMed: 17477822]

33. Matsuki H, et al. Both G3BP1 and G3BP2 contribute to stress granule formation. Genes Cells. 2013; 18:135–146. [PubMed: 23279204]

34. Tourrière H, et al. The RasGAP-associated endoribonuclease G3BP assembles stress granules. J Cell Biol. 2003; 160:823–831. [PubMed: 12642610]

35. Kedersha N, et al. G3BP-Caprin1-USP10 complexes mediate stress granule condensation and associate with 40S subunits. J Cell Biol. 2016; 212:845–860. [PubMed: 27022092]

36. Pendleton KE, et al. The U6 snRNA m^{6}A methyltransferase METTL16 regulates SAM synthetase intron retention. Cell. 2017; 169:824–835. [PubMed: 28525753]

37. Castello A, et al. Insights into RNA biology from an atlas of mammalian mRNA-binding proteins. Cell. 2012; 149:1393–1406. [PubMed: 22658674]

38. Baltz AG, et al. The mRNA-bound proteome and its global occupancy profile on protein-coding transcripts. Mol Cell. 2012; 46:674–690. [PubMed: 22681889]

39. Kwon SC, et al. The RNA-binding protein repertoire of embryonic stem cells. Nat Struct Mol Biol. 2013; 20:1122–1130. [PubMed: 23912277]

40. Irvine K, Stirling R, Hume D, Kennedy D. Rasputin, more promiscuous than ever: a review of G3BP. Int J Dev Biol. 2004; 48:1065–1077. [PubMed: 15602692]

41. Wei CM, Moss B. Nucleotide sequences at the N^6-methyladenosine sites of HeLa cell messenger ribonucleic acid. Biochemistry. 1977; 16:1672–1676. [PubMed: 856255]

42. Ke S, et al. A majority of m^{6}A residues are in the last exons, allowing the potential for 3′ UTR regulation. Genes Dev. 2015; 29:2037–2053. [PubMed: 26404942]

43. Linder B, et al. Single-nucleotide-resolution mapping of m^{6}A and m^{6}Am throughout the transcriptome. Nat Methods. 2015; 12:767–772. [PubMed: 26121403]

44. Tani H, et al. Genome-wide determination of RNA stability reveals hundreds of short-lived noncoding transcripts in mammals. Genome Res. 2012; 22:947–956. [PubMed: 22369889]

45. Myrick LK, Hashimoto H, Cheng X, Warren ST. Human FMRP contains an integral tandem Agenet (Tudor) and KH motif in the amino terminal domain. Hum Mol Genet. 2015; 24:1733–1740. [PubMed: 25416280]

46. Brown V, et al. Microarray identification of FMRP-associated brain mRNAs and altered mRNA translational profiles in fragile X syndrome. Cell. 2001; 107:477–487. [PubMed: 11719188]

47. Darnell JC, et al. FMRP stalls ribosomal translocation on mRNAs linked to synaptic function and autism. Cell. 2011; 146:247–261. [PubMed: 21784246]

48. Ascano M Jr, et al. FMRP targets distinct mRNA sequence elements to regulate protein expression. Nature. 2012; 492:382–386. [PubMed: 23235829]

49. Schwanhäusser B, Gossen M, Dittmar G, Selbach M. Global analysis of cellular protein translation by pulsed SILAC. Proteomics. 2009; 9:205–209. [PubMed: 19053139]

50. Visscher M, et al. Proteome-wide changes in protein turnover rates in *C. elegans* models of longevity and age-related disease. Cell Rep. 2016; 16:3041–3051. [PubMed: 27626671]

51. Chen CA, Shyu AB. Emerging themes in regulation of global mRNA turnover in cis. Trends Biochem Sci. 2017; 42:16–27. [PubMed: 27647213]

52. Costa M, Ochem A, Staub A, Falaschi A. Human DNA helicase VIII: a DNA and RNA helicase corresponding to the G3BP protein, an element of the ras transduction pathway. Nucleic Acids Res. 1999; 27:817–821. [PubMed: 9889278]

53. Anderson P, Kedersha N. Stress granules: the Tao of RNA triage. Trends Biochem Sci. 2008; 33:141–150. [PubMed: 18291657]

54. Scadden AD. Inosine-containing dsRNA binds a stress-granule-like complex and downregulates gene expression in trans. Mol Cell. 2007; 28:491–500. [PubMed: 17996712]

55. Kim SH, Dong WK, Weiler IJ, Greenough WT. Fragile X mental retardation protein shifts between polyribosomes and stress granules after neuronal injury by arsenite stress or in vivo hippocampal electrode insertion. J Neurosci. 2006; 26:2413–2418. [PubMed: 16510718]

56. Spruijt CG, et al. Dynamic readers for 5-(hydroxy)methylcytosine and its oxidized derivatives. Cell. 2013; 152:1146–1159. [PubMed: 23434322]

57. Qian K, et al. A simple and efficient system for regulating gene expression in human pluripotent stem cells and derivatives. Stem Cells. 2014; 32:1230–1238. [PubMed: 24497442]

58. Mali P, et al. RNA-guided human genome engineering via Cas9. Science. 2013; 339:823–826. [PubMed: 23287722]

59. Boersema PJ, Raijmakers R, Lemeer S, Mohammed S, Heck AJ. Multiplex peptide stable isotope dimethyl labeling for quantitative proteomics. Nat Protoc. 2009; 4:484–494. [PubMed: 19300442]

60. Pearson WR, Wood T, Zhang Z, Miller W. Comparison of DNA sequences with protein sequences. Genomics. 1997; 46:24–36. [PubMed: 9403055]

61. Trapnell C, Pachter L, Salzberg SL. TopHat: discovering splice junctions with RNA-Seq. Bioinformatics. 2009; 25:1105–1111. [PubMed: 19289445]

62. Corcoran DL, et al. PARalyzer: definition of RNA binding sites from PAR-CLIP short-read sequence data. Genome Biol. 2011; 12:R79. [PubMed: 21851591]

63. Heinz S, et al. Simple combinations of lineage-determining transcription factors prime cis-regulatory elements required for macrophage and B cell identities. Mol Cell. 2010; 38:576–589. [PubMed: 20513432]

64. Hinrichs AS, et al. The UCSC Genome Browser Database: update 2006. Nucleic Acids Res. 2006; 34:D590–D598. [PubMed: 16381938]

65. Huang W, Sherman BT, Lempicki RA. Bioinformatics enrichment tools: paths toward the comprehensive functional analysis of large gene lists. Nucleic Acids Res. 2009; 37:1–13. [PubMed: 19033363]

66. Supek F, Bošnjak M, Škunca N, Šmuc T. REVIGO summarizes and visualizes long lists of gene ontology terms. PLoS One. 2011; 6:e21800. [PubMed: 21789182]

67. Shannon P, et al. Cytoscape: a software environment for integrated models of biomolecular interaction networks. Genome Res. 2003; 13:2498–2504. [PubMed: 14597658]

68. Bray NL, Pimentel H, Melsted P, Pachter L. Near-optimal probabilistic RNA-seq quantification. Nat Biotechnol. 2016; 34:525–527. [PubMed: 27043002]

69. Cox J, Mann M. MaxQuant enables high peptide identification rates, individualized p.p.b.-range mass accuracies and proteome-wide protein quantification. Nat Biotechnol. 2008; 26:1367–1372. [PubMed: 19029910]

70. Wiśniewski JR, Zougman A, Mann M. Combination of FASP and StageTip-based fractionation allows in-depth analysis of the hippocampal membrane proteome. J Proteome Res. 2009; 8:5674–5678. [PubMed: 19848406]
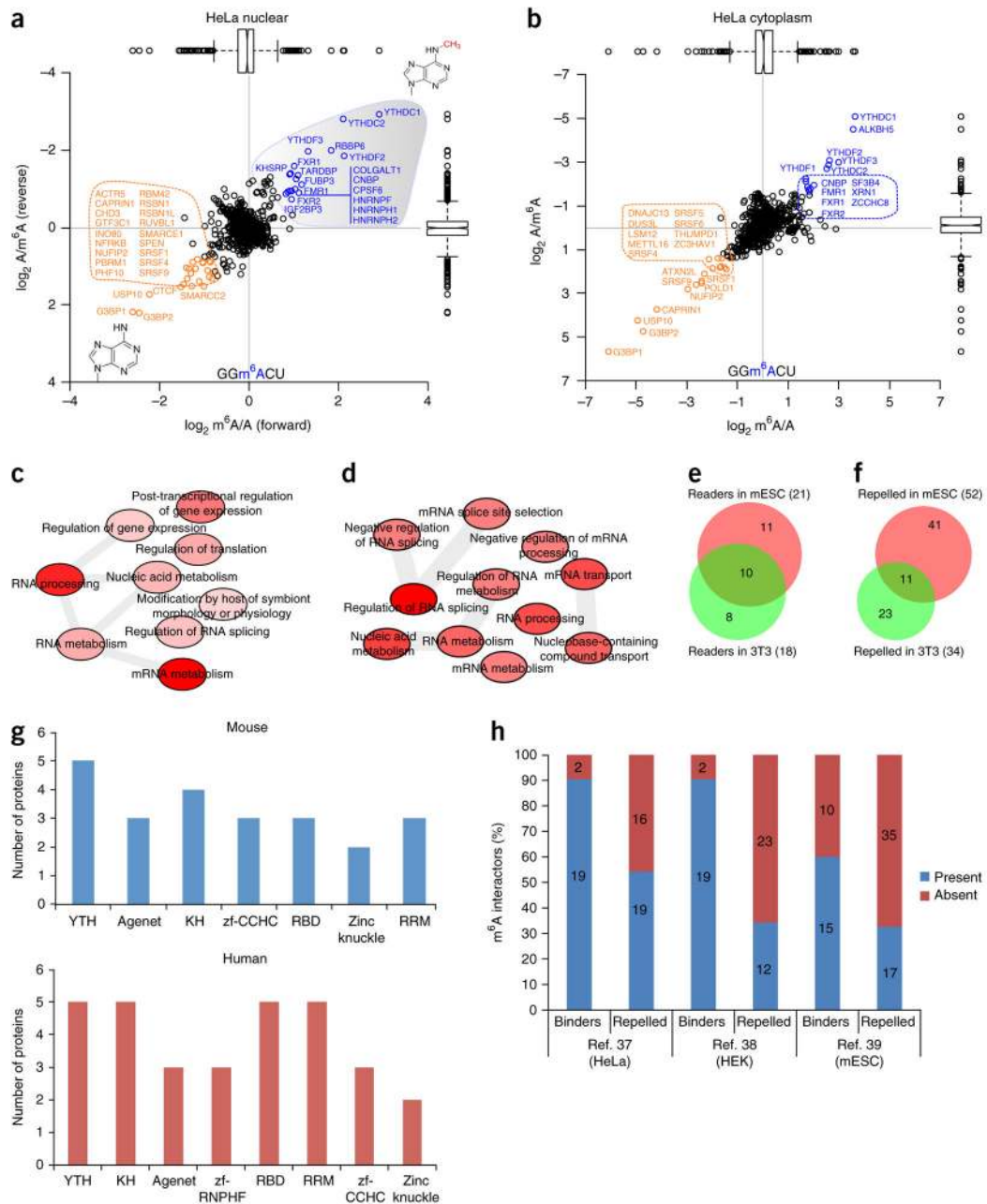
Figure 1.
A global m6A interactome. (**a**,**b**) Results of a SILAC-based m6A RNA pulldown in HeLa nuclear extract (**a**) and cytoplasmic lysates (**b**). m6A-interacting proteins are depicted in blue, repelled proteins are in orange, and background proteins are in black. We used a threshold of 1.5× the interquartile range to identify significant interactors. In the box plots, center lines indicate medians, box edges represent the interquartile range (IQR), and whiskers extend to ±1.5× the IQR; outlier values are shown as black circles. (**c**,**d**) GO-term enrichment analysis (Online Methods) of m6A readers (**c**) and repelled proteins (**d**) in HeLa cells. The relationships between various GO terms are depicted by gray bars. The intensity

of the red shading indicates the significance of the relationship (darker shading denotes greater significance). (**e**) The overlap between m[6]A readers identified in mESCs and differentiated cells (NIH 3T3). (**f**) The overlap between m[6]A-repelled proteins in mESCs and NIH 3T3 cells. The Venn diagrams summarize data obtained in three independent experiments. (**g**) Protein domains present in m[6]A interactors in mouse (top) and human (bottom) cells. (**h**) Many m[6]A interactors have also been identified in previously published *in vivo* mRNA-protein interaction studies[37–39]. Source data for **g** and **h** are available online. Proteomics data and GO enrichment analysis are presented in Supplementary Data Set 2.
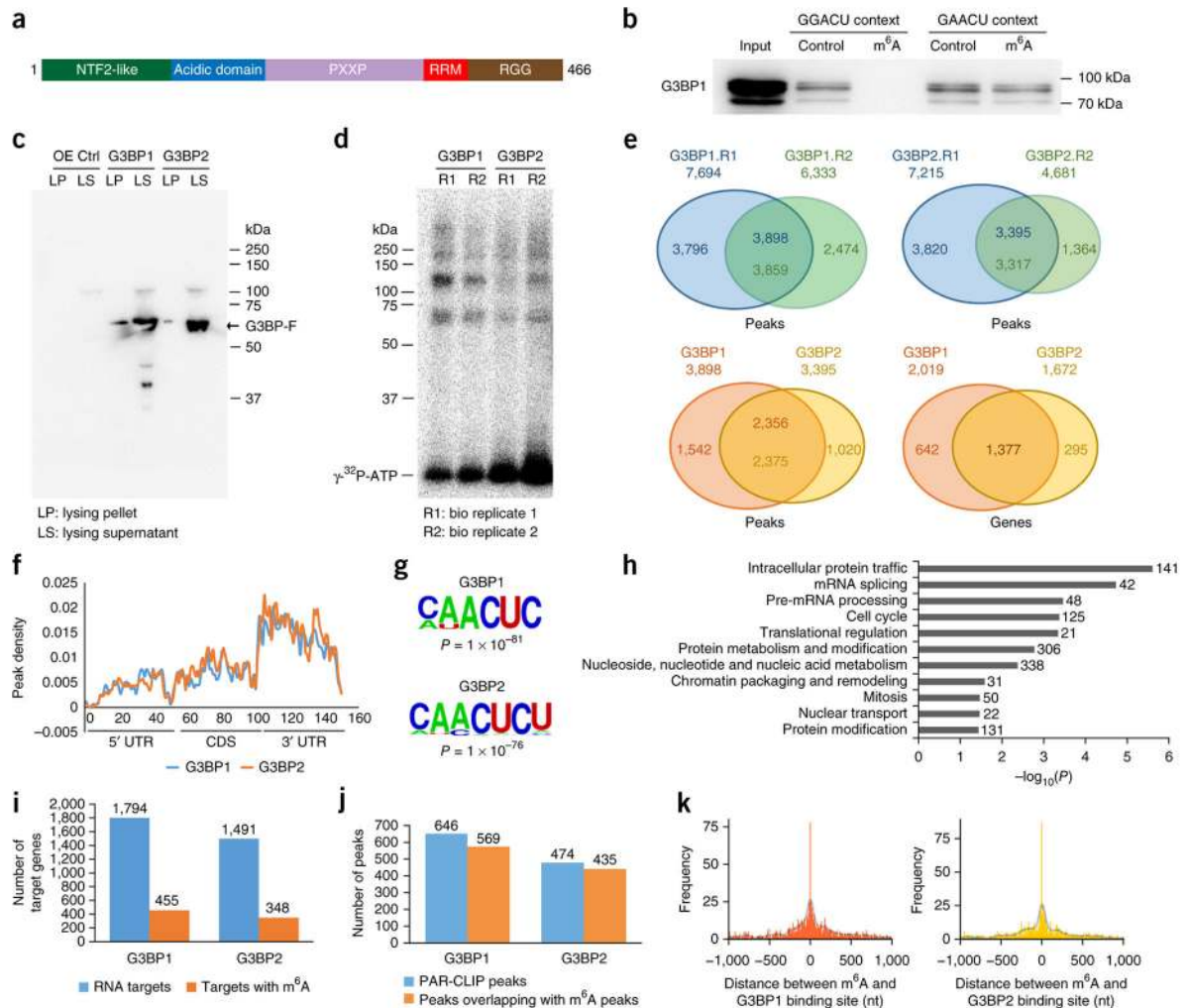
Figure 2.
G3BP1 and G3BP2 interact with thousands of transcripts. (**a**) The G3BP1 domain structure. (**b**) GST western blot showing RNA-sequence-context-dependent inhibition of GST-G3BP1 binding to RNA by m^{6}A. Molecular weights are indicated on the right. (**c**,**d**) RNA cross-link immunoprecipitation in HEK293 cells expressing either Flag-G3BP1 or Flag-G3BP2. Flag western blots (**c**) and radioactively labeled RNA-protein complexes (**d**) are shown. OE, overexpression; Ctrl, control. (**e**) Common peaks between PAR-CLIP biological replicates 1 and 2 for G3BP1 (top left) and G3BP2 (top right), and comparisons between G3BP1 and G3BP2 peaks (bottom left) and target genes (bottom right). (**f**) Metagene profiles of G3BP1 and G3BP2 distribution across the transcriptome. (**g**) The most enriched consensus sequences of G3BP1 (top) and G3BP2 (bottom) on mRNA; *P* values were determined as described in the Online Methods. (**h**) The most significantly enriched GO terms among G3BP1 target genes. The numbers to the right of the bars represent the number of genes in that GO term. (**i**) The number of G3BP1 and G3BP2 peaks that overlap with m^{6}A peaks among m^{6}A-containing mRNAs. (**j**) The number of G3BP1 and G3BP2 peaks on m^{6}A-containing mRNAs that overlap with m^{6}A. (**k**) The distribution of G3BP1 (left) and G3BP2

(right) relative to m^{6}A sites at single-nucleotide resolution[43]. The distance between PAR-CLIP peaks and m^{6}A sites was counted in 10-nucleotide bins. A Gaussian kernel smoothing over the histogram is plotted as a transparent black line. The uncropped blot image for **b** is shown in Supplementary Data Set 1. Source data for **i** and **j** are available online. G3BP1 and G3BP2 PAR-CLIP data and related GO term enrichment analysis are presented in Supplementary Data Set 3.
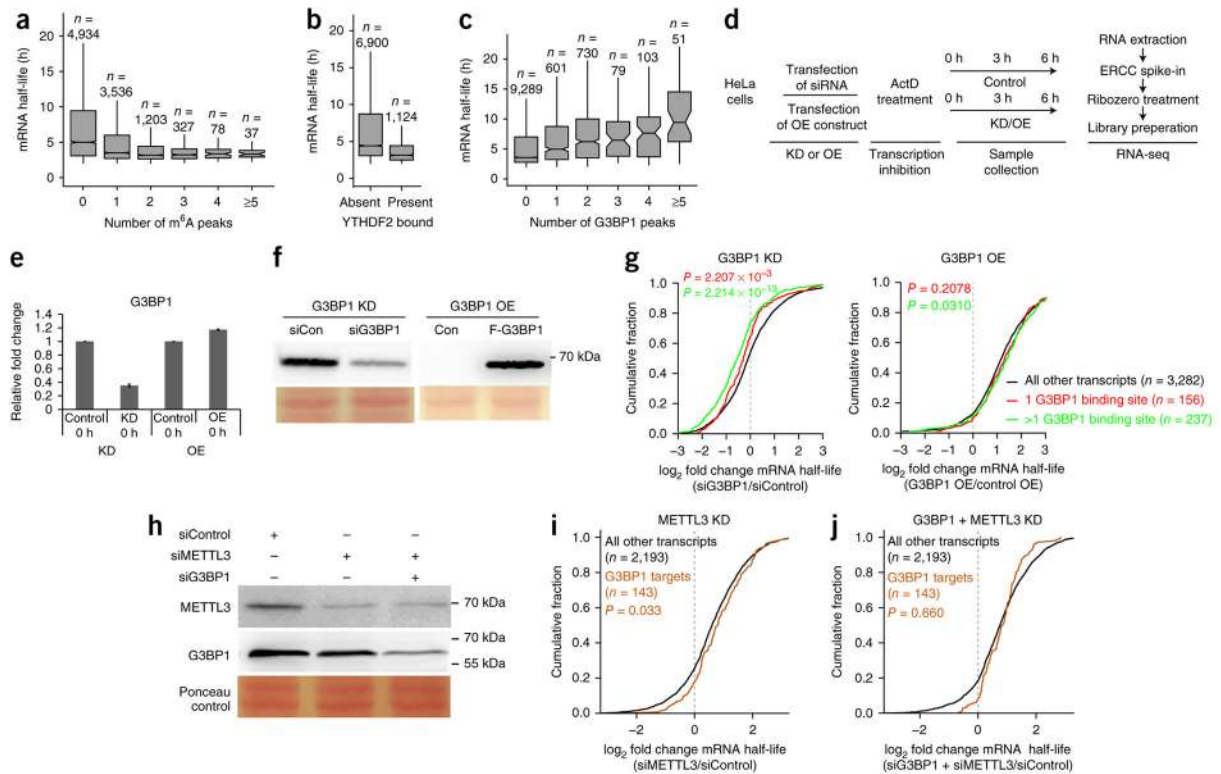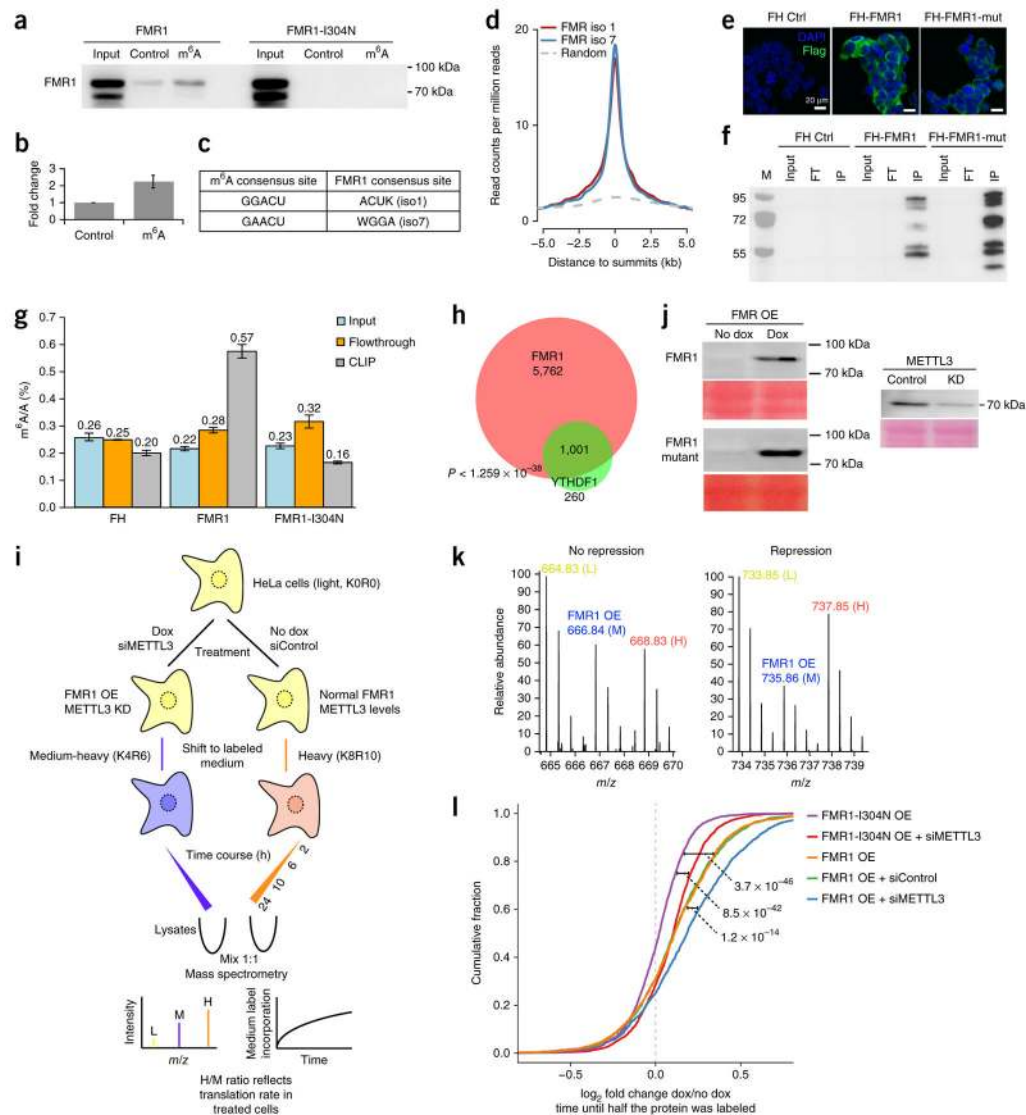
Figure 3.
G3BP1 protects target mRNAs from degradation. (**a**) The correlation between the number of m[6]A peaks[19] on mRNA molecules and mRNA half-life[44]. (**b**) The correlation between YTHDF2 mRNA binding[19] and mRNA stability. (**c**) The correlation between G3BP1 mRNA binding and target gene transcript stability[44]. In **a–c**, n represents the number of genes, center lines in box plots indicate medians, box edges represent the interquartile range, and whiskers extend to $\pm 1.5\times$ the interquartile range; outlier values are not shown. (**d**) mRNA half-life measurements after G3BP1 knockdown (KD) or overexpression (OE). ActD, actinomycin D. (**e**) qPCR analysis of G3BP1 levels after protein knockdown or overexpression. GAPDH was used to normalize expression. Data are shown as the mean ± s.e.m.; $n = 3$ independent experiments. (**f**) Western blots depicting knockdown and overexpression of G3BP1. Ponceau-stained protein bands are shown as loading controls. Con, control plasmid expressing Flag tag. (**g**) Cumulative distribution function plots showing the effect of G3BP1 knockdown on target genes. The $\log_2$ fold changes in mRNA half-life were grouped and analyzed on the basis of the number of G3BP1-binding sites on each transcript. P values were calculated by two-sided Mann–Whitney U test. (**h**) Western blots depicting knockdown of METTL3 and G3BP1. Ponceau-stained protein bands are shown as loading controls. (**i**) A cumulative distribution function plot showing the effect of METTL3 knockdown on G3BP1 target genes. (**j**) A cumulative distribution function plot showing the effect of combined G3BP1 and METTL3 knockdown on G3BP1 target genes. $\log_2$ fold changes were grouped and analyzed as described for **g**. Uncropped blot images for **f** and **h** are shown in Supplementary Data Set 1. A summary of mRNA half-lives as determined by RNA-seq analysis is presented in Supplementary Data Set 4.

Figure 4.

FMR1 preferentially binds to m[6]A-containing mRNA *in vitro* and *in vivo* and affects the translation of its targets. (**a**) Western blots showing preferential m[6]A binding by recombinant GST-FMR1 *in vitro*. (**b**) Quantification of FMR1 binding to control and m[6]A probes (data are shown as mean ± s.e.m.; $n = 3$ independent experiments). (**c**) Predominant consensus sequences for m[6]A[9,10] and consensus mRNA-binding sites for FMR1 isoforms 1 and 7 (ref. 48). (**d**) Visualization of binding of FMR1 isoforms 1 and 7 to mRNA relative to known m[6]A sites on mRNA[10,48]. Randomized peaks were generated from the transcriptome and used as a control as described in the Online Methods. (**e**) Immunofluorescence analysis of the expression of Flag-HA (FH)-tagged FMR1 isoform 1 and Flag-HA-tagged FMR1 isoform 1 I304N mutant (mut) in HEK293T cells. (**f**) RNA cross-linking and immunoprecipitation in lysates from HEK293 cells expressing either Flag-HA-tagged FMR1 or Flag-HA-tagged FMR1-I304N, using anti-Flag. IP, immunoprecipitate; FT, flow-through; M, molecular weight ladder. (**g**) Representative LC-MS quantification showing enrichment

of m^{6}A in Flag-HA-tagged FMR1–bound mRNA. Error bars represent the range; $n = 2$ independent experiments. (**h**) The overlap between FMR1 (ref. 48) and YTHDF1 target transcripts[22]. (**i**) A schematic representation of the pulsed SILAC workflow. Dox, doxycycline. (**j**) Western blots showing the results of METTL3 knockdown and inducible FMR1/FMR1 mutant protein expression in HeLa cells. Ponceau-stained protein bands are shown as loading controls. (**k**) Representative peptide spectra showing SILAC label incorporation for a peptide belonging to a protein whose translation rate is not affected by FMR1 overexpression (left) and a peptide belonging to a protein that is translationally repressed by FMR1 overexpression (right) (compare the incorporation of medium-heavy (M) and heavy (H) label in the two plots). (**l**) A cumulative distribution function plot showing the effect of METTL3 knockdown (siMETTL3), FMR1 overexpression, and FMR1-I304N overexpression on translation rates in HeLa cells. We used the time until half the protein was labeled as a proxy for the translation rate (Online Methods). A summary of the proteomics data from the pulsed SILAC analyses is provided in Supplementary Data Set 5. Uncropped blot images for **a**, **f** and **j** are shown in Supplementary Data Set 1. Source data for **g** are available online.